Near and far-field tsunamigenic effects on the Z-component of the geomagnetic field during the Japanese event, 2011

V. Klausner,[1] Esfhan A. Kherani,[2] and Marcio T. A. H. Muella,[1]

Corresponding author: V. Klausner, Physics and Astronomy, Vale do Paraiba University, Av. Shishima Hifumi, 2911, IP&D, CEP 12244-000, São José dos Campos, SP, Brazil (viklausner@gmail.com)

[1]Vale do Paraiba University, Physics and Astronomy, São José dos Campos, SP, Brazil.

[2]National Institute for Space Research, São José dos Campos, SP, Brazil.

This article has been accepted for publication and undergone full peer review but has not been through the copyediting, typesetting, pagination and proofreading process, which may lead to differences between this version and the Version of Record. Please cite this article as doi: 10.1002/2015JA022173

Abstract. In this work, we examine the vertical component (Z) of the geomagnetic field observed by ground-based observatories during the tsunami event which happened on 11th March, 2011. For this event, we have selected nine magnetic observatories distributed along the tsunami passage, covering up to 3000 km epicentral distance. The travel-time diagram of the magnetic disturbances is constructed and compared with the simulated tsunami travel-time diagram. From this comparison, we identify the amplified magnetic disturbances appearing during the tsunami arrival in the vicinity of these observatories. Moreover, mean absolute percentage error map is constructed to examine the cross-correlations among different observatories and the amplified disturbances are found to be highly correlated. These features suggest that the amplified disturbances are tsunamigenic in nature. These results are in confirmation with the previous near-field studies, as well they shed new insight into the tsunamigenic magnetic disturbances on near and far-field distances from the epicenter.

1. Introduction

Perturbations in the geomagnetic field induced by the tsunami have been observed by several authors [*Balasis and Mandea*, 2007; *Manoj et al.*, 2011; *Toh et al.*, 2011; *Utada et al.*, 2011; *Klausner et al.*, 2014] and modeled [*Tyler*, 2005; *Kherani et al.*, 2012; *Minami and Toh*, 2013; *Zhang et al.*, 2014; *Kherani et al.*, 2015] in the previous literature.

Manoj et al. [2011] observed at three different observatories the geomagnetic disturbances caused by the tsunami of moderate level that occurred in the Pacific ocean during February 2010 by the Chilean earthquake of magnitude 8.8. Their observations presented a variation of 1 nT in the vertical component of the magnetic field (Z) during the time corresponding to the tsunami effects. Movement of electrically conducting sea-water through the geomagnetic field generates an electromotive force that induces electric fields, electric currents and secondary magnetic fields. In other words, tsunamis can produce perturbations in the Earth's magnetic field by electro-magnetic induction [see *Manoj et al.*, 2011, and references therein]. In addition, gravity waves are generated by the displacement of the atmosphere due to the earthquake and the tsunami wave propagation. These waves propagate in the ionosphere inducing magnetic fields, and also they produce perturbations in the Earth's magnetic field. This mechanism was first proposed by *Heki and Ping* [1998].

Klausner et al. [2014] examined the 27th February, 2010 Chilean tsunami using an improved methodology based on wavelet techniques applied to the Z-component of magnetogram data, when the previous study of *Manoj et al.* [2011] employed mainly visual

inspection. Their work evaluated the wavelet techniques as an effectively tool that could be used to characterize the tsunamigenic contributions to the geomagnetic field.

In this work, we focus on the survey of geomagnetic variations induced by the Japanese tsunami event of 11th March, 2011 that occurred at 05 : 46 UT with 8.9 M_w and whose epicenter was located at Lat. 38.3° and Long. 142.4°, near to the east coast of Honshu, at 24km depth. For this tsunami, *Kherani et al.* [2012] have reported the near-field tsunamigenic magnetic disturbances in the Z-component covering up to 400 km epicentral distance, and explained them as the ionospheric current contribution arising from the forcing from the tsunamigenic acoustic gravity waves (AGWs). *Utada et al.* [2011] have also reported the near-field tsunamigenic magnetic disturbances in all three components along the east coast of Honshu. While these studies mentioned above provided detailed aspects of near-field tsunamigenic disturbances, their presence in the far-field is yet to be verified. In the present study, we focus on identifying both near and far-field tsunamigenic disturbances arising from ionospheric currents. Previous work done by *Klausner et al.* [2014] has identified the tsunamigenic disturbances in the vertical component of the geomagnetic field. Likewise, presenting all three components of magnetic disturbances during the Japanese tsunami (2011), *Kherani et al.* [2012] have found the tsunamigenic disturbances mainly in Z-component. Therefore, we focus on Z-component of the geomagnetic field to search for the tsunamigenic disturbances.

The present paper is organized as follows: in Section 2, we describe the magnetic data and methodology adopted for the analysis; in Section 3, the results are presented and discussed. Finally, in Section 4, we summarize the main results and present the conclusions.

2. Magnetic Data

It is well-known that the intensity of the geomagnetic disturbance in each day is described by indices, and the variation of these indices is used to distinguish the days as quiet or disturbed. There are different indices that can be used depending on the character and the latitude influences in focus. In this work, the SYM-H index was used to identify periods of disturbed geomagnetic field conditions. The SYM-H is a minutely index, while Dst index is a hourly index. The index most used in low latitudes is the Dst, very similar to the SYM-H index but with lower resolution (1 hour). Both of these indices represent the variations of the H-component due to changes of the ring current [*Gonzalez et al.*, 1994].

On day of the Japanese tsunami (11th March, 2011) occurred a geomagnetic disturbance which corresponded to a moderate storm with minimum Dst = −82nT at 06 : 00 UT, and a second energy injection at 18 : 00 UT with minimum Dst = −67nT at 22 : 00 UT. Therefore, this day is classified as a geomagnetically disturbed day.

To examine the tsunamigenic disturbances, we analyze the magnetic data from nine chosen observatories belonging to the INTERMAGNET programme and Geospatial Information Authority of Japan (GIS). These observatories are: CBI, ESA, HAR, GUA, KAK, KNY, MMB, OTA, and TTK (see Table 1). Excluding GUA, all the other magnetic observatories were also used by *Utada et al.* [2011] to study the geomagnetic responses to this tsunami. Figure 1 displays the magnetic observatories distributed across the ocean and the TTT (tsunami travel time) map. In both graphics, the arrows denoted by 1 and 3 represent the directions along the coast while the arrow denoted by 2 represents the direction along the tsunami.

At first, we present the data filtered below 5000 seconds that covers the response periods of the atmospheric wave induced ionospheric currents [*Occhipinti et al.*, 2006, 2008, 2011; *Rolland et al.*, 2010; *Kherani et al.*, 2012]. This cutoff period is used to exclude the ambient magnetic field variation arising from the Sq current system. In addition, based on simulation study of tsunamigenic magnetic disturbances [*Kherani et al.*, 2012] that shows the spectral peak between 3–61 minutes, we narrow down the filter between 20–40 minutes and complement the results by constructing travel-time diagram (TTD) or Keogram as done by *Kherani et al.* [2012]. We also present the mean absolute percentage error (MAPE) map to identify the tsunamigenic signatures in the Z-component. These TTD and MAPE map are constructed by distributing the time series of Z-component in space, based on the geographic locations of a few magnetic observatories as we will show further.

While plotting these dataset, we also plot the tsunami travel-time (TTT) diagram. This tsunami event was simulated using the model developed by *Sladen et al.* [2007]; *Sladen and Hérbert* [2008]. The TTT diagram provides the reference propagation characteristics nearest to each magnetic observatory location, based on which, we interpret the filtered data and search for tsunamigenic disturbances. Here, the tsunami arrival times do not correspond to the tsunami arrival time to the ground land magnetic observatories, but correspond to the locations of tide gauges simulated along coastlines (see Table 2). By analyzing Table 2, it is possible to notice that the maximum location difference between tsunami arrival and observatories is less than 50 km, so the errors in the estimated tsunami time arrival due to the location difference between magnetic field observations and sea surface displacement observations can be up to $\sim \pm 4$ minutes, assuming the tsunami

velocity of 200 m/s. Therefore, the tsunami arrival nearest to the observatories is taken as an approximate reference having maximum error observed at three different observatories the geomagnetic disturbances caused by the tsunami of moderate level that occurred in the Pacific ocean during February 2010 by the Chilean earthquake of magnitude 8.8.in location difference of about 50 km which corresponds to 4 minute time difference, if the tsunami has arrived exactly at the observatory location. This error is well within the time duration of ∼10–50 minutes required for the tsunami-ionosphere coupling through the atmosphere [*Kherani et al.*, 2012] and therefore the tsunamigenic disturbances due to the ionospheric currents can be identified based on arrival time of tsunami nearest to each observatory. On the other hand, this error exclude the possibility of identifying the tsunamigenic disturbances arising from the oceanic currents since they appear in phase or out of phase with the tsunami appearing within ±4 minutes with the tsunami arrival [*Tyler*, 2005; *Minami and Toh*, 2013; *Sugioka et al.*, 2014].

3. Results and Discussion

In Figure 2, on the left, from top to bottom, the panels correspond to magnetic observatories of MMB, ESA, HAR, KAK, OTA, TTK, KNY, CBI, and GUA, respectively. Each panel displays the corresponding preprocessing magnetogram which was applied a high-pass filter with a cutoff period of 5000s (Z-component). The filter applied here was the same used by *Zhang et al.* [2014], and also covers the spectral peak between 3–61 minutes detected by *Kherani et al.* [2012]. The tsunami wave-field, obtained using the tsunami simulation model [*Sladen et al.*, 2007; *Sladen and Hérbert*, 2008], is also superimposed (black color) at each station in this plot. On the right, spectral analysis using gapped wavelet technique (GWT) is presented for each respective magnetic observatory.

The GWT can be used in the analysis of non-stationary signal to obtain information on the frequency or scale variations and to detect its structures localization in time and/or in space. It is possible to analyze a signal in a time-scale plane, the so called, wavelet scalogram. In analogy with the Fourier analysis, the square modulus of the wavelet coefficient, $|W(a,b)|^2$, is used to provide the energy distribution in the time-scale plane. The advantage of GWT is the reduction of the effects of the presence of gaps in time series and the boundary effects due to the finite length of time series [see *Klausner et al.*, 2014, for more details]. This technique was employed by *Klausner et al.* [2014] and it shows a great potential to detect tsunamigenic magnetic signals with a period range from 2 to 64 minutes which can be associated to gravity wave propagation induced by tsunamis.

From this Figure, we note the development of spectral peak within 1 hour after the tsunami arrival at almost all locations, except KNY which is not located in the direction of maximum tsunami energy propagation. These spectral peaks reside between 16–128 minutes, and they follow similar propagation pattern between observatories as the simulated tsunami propagation shown in the right panel. To confirm this aspect, we complement Figure 2 by constructing travel-time diagram (TTD) in Figure 3.

In Figure 3 from bottom to top, the TTD of the Japanese tsunami is presented using the tsunami propagation direction 1, 2 and 3, respectively. In the following, we describe each panel one after another. The wave front direction number 1 is parallel to the Japanese coast on the west-southwest direction, and in this case the magnetic observatories used are KAK, TTK and KNY. The filtered data is plotted in the blue color. The TTT diagram of the wave-field, is also superimposed (dashed black color). On the filtered magnetograms, we search for wave packets with amplified magnitude of magnetic field around the tsunami

arrival time with ±4 minutes error, and if they exist, we highlight them (red color) to obtain their propagation characteristics. We are able to identify amplified wave packets at KAK, TTK and KNY respectively at 6 : 30 – 7 : 00, 7 : 30 – 8 : 00 and 9 : 00 – 9 : 30 UT hours, and they are denoted by ellipses. The direction 2 is towards the open sea waters, and in this case the magnetic observatories used are OTA, CBI and GUA. From this TTD on direction 2, the wave packets are identified following the same strategy as described in the context of TTD on direction 1. In this case, we are able to identify similar wave packets at OTA, CBI and GUA respectively at 6 : 30 – 7 : 00, 7 : 30 – 9 : 00 and 9 : 30 – 10 : 00 UT hours. It is possible to notice that these ellipses are corresponding to the spectral packets identified in Figure 2. This suggests that the identified wave packets have propagation characteristics similar to the tsunami wavefront propagation, and it ensures that these wave packets are tsunamigenic disturbances. The direction 3 is parallel to the Japanese coast on the west-northward direction, and the magnetic observatories used are ESA and MMB. Once more, we search for amplified wave packets around the tsunami arrival time. In this case, we are able to identify similar wave packets at ESA and MMB respectively at 5 : 50 – 6 : 30 and 6 : 00 – 6 : 30 UT hours. The same as noticed on direction 2, it is also possible to notice on the direction 3 that the ellipses are corresponding to the spectral packets identified in Figure 2. It can be said again that the identified wave packets have propagation characteristics similar to the tsunami wavefront propagation what ensures that these wave packets are tsunamigenic disturbances.

On all three studied tsunami directions, we also note the presence of largest amplitude/N-shaped pulse inside these identified wave packets (marked by red color). For the Japanese tsunami, the co-seismic magnetic disturbances of such characteristics

are recently reported by *Kherani et al.* [2012]. Therefore, we identify wave packets and N-shaped amplified pulses as of tsunamigenic nature. Both oceanic [*Tyler*, 2005] and acoustic gravity wave (AGW) driven ionospheric currents [*Heki and Ping*, 1998; *Kherani et al.*, 2012] associated to the tsunami are known to excite the magnetic disturbances with similar propagation characteristics as the tsunami waves. At this point, the relative contribution of oceanic currents and of ionospheric currents to the identified magnetic disturbances will remain an unresolved issue since the time error of ±4 minutes due to the location difference between tsunami arrival and observatories masks the oceanic current contribution. More importantly, the numerical experiment by *Zhang et al.* [2014] clearly shows that Z-component variation of oceanic current origin can not explain the N-shaped variation at ESA. Therefore, the N-shaped pulses in Figure 3 are not of oceanic current origin. On the other hand, the numerical experiment by *Kherani et al.* [2012] shows that tsunamigenic AGWs driven ionospheric currents which can give rise to the N-shaped Z-component disturbances appearing within 10–40 minutes from the tsunami arrival. Therefore, these pulses are tsunamigenic in nature arising most possibly from the ionospheric currents.

In addition to the construction of TTD in 3 directions together with the simulated tsunami as a reference, identification of tsunamigenic disturbances in the far-field locations such as GUA and KNY are the important results of the present work. In these two far-field locations, the disturbances are identified 3 hours after the tsunami initiation. Identification of tsunamigenic disturbances at such later time is possibly reported for the first time. Moreover, the TTD helps to interpret the tsunamigenic disturbances more accurately. For example, at TTK, two peaks are noted: one around 6:00 hours and another

around 7:30 hours. The later one is identified as the tsunamigenic since it occurs at the time of tsunami arrival at TTK. The first peak around 6:00 hours occurs much earlier than the tsunami arrival and is possibly related to the seismogenic magnetic disturbances as interpreted by *Utada et al.* [2011]. The magnetic disturbances at GUA and KNY also present similar scenario where two peaks, one between 6-7 hours and another around 9:00 hours are noted. The later peak is tsunamigenic as interpreted by us in the present study while the first one is possibly seismogenic as interpreted by *Utada et al.* [2011] for KNY. This kind of interpretation could only be possible by constructing the TTD, and, by these reasons, the TTDs are important tools to identify the tsunamigenic disturbances.

To ensure the identification of tsunamigenic disturbances, we create a MAPE map between the all the magnetic observatories. We considered as positive radial distances from the epicenter the observatories along the tsunami wave front propagation with maximum energy, in this case, ESA, MMB, CBI and GUA. The wave packet induced by the tsunami for the nearest observatory (HAR) to the epicenter was used to construct the fitted time series values for each piece of the Z-component series, filtered with a bandpass with periods between 20 and 40 minutes with the same length of the wave packet. Then, it was shifted forward with a step of 1 minute, and the process was repeated over the entire data set. Figure 4 shows the MAPE map considering same range of time period used in the TTD and radial distance in kilometers from each magnetic observatory to the epicenter. The mean absolute percentage error (MAPE) was calculated as $MAPE = \frac{1}{N}\sum_{n=1}^{N}|\frac{A_t - B_t}{A_t}|$ where N is the length tsunamigenic magnetic induction (adopted $N = 60$ minutes), A_t is the magnetogram of the closest magnetic observatory to the epicenter, B_t is each other observatory used in this work, and t is the length of a day ($1 \leq t \leq 1440$ minutes). We

note the amplification of MAPE in the vicinity of tsunami arrival time such that this amplified MAPE contours follows the tsunami propagation. The TTD analysis together with the MAPE analysis ensure that the identified wave-packets and N-shaped pulses within it in the Figure 3 are of tsunamigenic nature.

We point out that we are not discussing any Rayleigh and/or acoustic disturbances in Figure 3. These features are analyzed in the work done by *Klausner et al.* [2015] using the same dataset and directions used here, and they detect similar wave packets in far-field distances up to 3 hours in advance of the tsunami arrival. Also, Ahead-of-Tsunami-Traveling-Ionospheric-disturbances (ATIDs) has been simulated by *Kherani et al.* [2015] which propagate ahead of the principal tsunami wave-front arriving $\sim 20 - -60$ minutes in advance. To detect these disturbances are beyond the scope of this paper. In this paper, we focus on the disturbances seen within 1 hour from the tsunami arrival. In Figure 3, we clearly note disturbances at each observatories occurring within 1 hour from the tsunami arrival and follow same propagation pattern as the tsunami. Therefore, they are identified as the tsunamigenic disturbances. *Kherani et al.* [2012] reported the tsunamigenic disturbances within 400 km from the epicenter distance while the present work reports the tsunamigenic disturbances beyond 400 km covering as far as 3000 km distance. This kind of results could only be possible by constructing the TTD and therefore the TTDs are important tools to identify the tsunamigenic disturbances.

We associate these amplified pulses in Figure 3 as dominantly of ionospheric current origin. For the CBI, this outcome is consistent with the finding of *Zhang et al.* [2014] who noted the simulated disturbances of oceanic currents. Since their simulation did not

include ionospheric dynamics, obviously they will see only oceanic current contribution, and any contribution from ionospheric currents.

4. Conclusion

In this work, we report the tsunamigenic magnetic disturbances identified from 9 ground magnetometer measurements during Japan 2011 tsunami. In order to identify the tsunamigenic disturbances, we adopt the gapped wavelet methodology complemented by the TTDs and MAPE map which are shown to be effective tools recently [*Kherani et al.*, 2012; *Klausner et al.*, 2014]. The following results can be highlighted from the present study:

1. The gapped wavelet methodology alone can identify the tsunamigenic disturbances for near-field observatories. However, for far-field observatories, this methodology alone does not identify, beyond any doubt, the tsunamigenic disturbances.

2. When the gapped wavelet analysis is complemented by the TTDs or keograms and MAPE map, the tsunamigenic disturbances are identified up to the locations as far as 3000 km from the epicenter.

3. In TTD and MAPE map, the wave packets of one hour are observed during the tsunami arrival time and they are found to have propagation characteristics similar to the principal tsunami wavefront. On this basis, they are identified as the tsunamigenic packets of disturbances.

4. Inside these tsunamigenic packets, amplified N-shaped pulses are identified and they are argued as owing to ionospheric currents arising from the tsunami ionosphere coupling through AGWs as recently shown by *Kherani et al.* [2012].

These results are encouraging and suggest that the Z-component monitoring could potentially be used in concern with ionospheric measurements [*Occhipinti et al.*, 2006, 2008, 2010, 2013; *Rolland et al.*, 2010; *Galvan et al.*, 2012] and/or sea-floor electric field measurements (see *Manoj et al.* [2010] and references therein) to calibrate tsunami models and to provide additional information about the tsunami propagation.

Acknowledgments. V. Klausner wishes to thank CAPES for the financial support of her PhD (CAPES – grants 465/2008) and her Postdoctoral research within the Programa Nacional de Pós-Doutorado (PNPD – CAPES) and (FAPESP – grants 2011/21903-3, 2011/20588-7 and 2013/06029-0). The authors would like to thank the National Oceanic and Atmospheric Administratio (NOAA), Geospatial Information Authority of Japan (GIS) and the International Real-time Magnetic Observatory Network (INTERMAGNET) for the datasets used in this work. The NOAA tsunami-travel time map was generated by MOST (Method of Splitting Tsunami) model and distributed by NOAA Center for Tsunami Research (http://nctr.pmel.noaa.gov/model.html). The GIS data were obtained freely from the GIS server (html://vldb.gsi.go.jp/sokuchi/geomag/index-e.html). The INTERMAGNET data were downloaded from INTERMAGNET website (http://www.intermagnet.org). Also, the authors would like to thank Dr. Anthony Sladen for the tsunami simulated data used here and Dr. F. C. de Meneses for the filtered data.

References

Balasis, G., and M. Mandea (2007), Can electromagnetic disturbances related to the recent great earthquakes be detected by satellite magnetometers?, *Tectonophysics*, *431*, 173–195.

Heki, K., and J. Ping (1998), Directivity and apparent velocity of the coseismic ionospheric disturbances observed with a dense GPS array, *Earth and Planetary Science Letters*, *236*(3-4), 845–855.

Galvan, D. A., A., Komjathy, M. P., Hickey, P., Stephens, J., Snively, Y. T., Song, M. D., Butala, and A. J., Mannucci (2012), Ionospheric signatures of Tohoku-Oki tsunami of March 11, 2011: Model comparisons near the epicenter. *Radio Science*, *47*(4), RS4003.

Gonzalez, W. D., J. A., Joselyn, Y., Kamide, H. W., Kroehl, G., Rostoker, B. T., Tsurutani, and V. M., Vasyliunas (1994), What is a geomagnetic storm? *Journal of Geophysical Research*, *99*(A4), 5771–5792.

Kherani, E. A., P. Lognonné, H. Hébert, L. Rolland, E. Astafyeva, G. Occhipinti, P. Coïsson, D. Walwer, E. R. de Paula (2012), Modelling of the total electronic content and magnetic field anomalies generated by the 2011 Tohoku-Oki tsunami and associated acoustic-gravity waves, *Geophysical Journal International*, *191*(3), 1049–1066.

Kherani, E. A., L. Rolland, P. Lognonné, A. Sladen, V. Klausner, and E. R. de Paula (2015), Traveling ionosphere disturbances propagating ahead of the Tohoku-Oki tsunami: a case study, *Geophysical Journal International*, accepted 2015 November 15, in press.

Klausner, V., O. Mendes, M. O. Domingues, A. R. R. Papa, R. H. Tyler, P. Frick, and E. A. Kherani (2014), Advantage of wavelet technique to highlight the observed geomagnetic perturbations linked to the Chilean tsunami (2010) *Journal of Geophysical Research: Space Physics*, *119*(4), 3077–3093.

Klausner, E. A. Kherani and M. T.A. H. Muella (2015), Rayleigh and acoustic gravity waves detection on magnetograms during the Japanese Tsunami, 2011, *Arxiv*,

abs/1508.00428, http://arxiv.org/abs/1508.00428

Manoj, C., A. Kuvshinov, S. Neetu, and T. Harinarayana (2010), Can undersea voltage measurements detect tsunamis?, *Earth, Planets and Space*, *62*(3), 353–358.

Manoj, C., S. Maus, and A. Chulliat (2011), Observation of Magnetic Fields Generated by Tsunamis, *EOS, Transactions American Geophysical Union*, *92*(2), 13–14.

Minami, T., and H. Toh (2013), Two-dimensional simulations of the tsunami dynamo effect using the finite element method, *Geophysical Research Letters*, *40*, 4560–4564.

Occhipinti, G., P. Lognonné, E. A. Kherani, and H. Hébert (2006), 3D Waveform modeling of ionospheric signature induced by the 2004 Sumatra tsunami. *Geophysical Research Letters*, *33*, L20104.

Occhipinti, G., A. Kherani , P. Lognonné (2008), Geomagnetic dependence of ionospheric disturbances induced by tsunamigenic internal gravity waves. *Geophysical Journal International*, *173*(3), 753–765.

Occhipinti, G., P. Dorey, T. Farges, and P. Lognonné (2010), Nostradamus: The radar that wanted to be a seismometer. *Geophysical Research Letters*, *37*(18), L18104.

Occhipinti, G., P. Coisson, J. J. Makela, S. Allgeyer, A. Kherani, H. Hébert, and P. Lognonné (2011), Three-dimensional numerical modeling of tsunami-related internal gravity waves in the Hawaiian atmosphere. *Earth Planets Space*, *63*(7), 847–851.

Occhipinti, G., L. Rolland, P. Lognonné, S. Watada (2013), From Sumatra 2004 to Tohoku-Oki 2011: The systematic GPS detection of the ionospheric signature induced by tsunamigenic earthquakes. *Journal of Geophysical Research: Space Physics*, *118*(6), 3626–3636.

Rolland, L., G. Occhipinti, P. Lognonné, and A. Loevenbruck (2010), Ionospheric gravity waves detected offshore Hawaii after tsunamis, *Geophysical Research Letters*, *37*(17), L17101.

Rolland, L., P. Lognonné, E. Astafyeva, E. A. Kherani, N. Kobayashi, M. Mann, and H. Munekane (2011), The resonant response of the ionosphere imaged aftes the 2011 Tohoku-Oki earthquake *Earth Planets Space*, *63*, 853–857.

Sladen, A., H. Hébert, F. Schindelé, and D. Reymond (2007), Evaluation of far-field tsunami hazard in French Polynesia based on historical data and numerical simulations. *Natural Hazards and Earth System Science*, *7* (2), 195–206.

Sladen, A., and H. Hébert (2008), On the use of satellite altimetry to infer the earthquake rupture characteristics: application to the 2004 Sumatra event. *Geophysical Journal International*, *172* (2), 707–714.

Sugioka, H., Y. Hamano, K. Baba, T. Kasaya, N. Tada, and D. Suetsugu (2014), Tsunami: Ocean dynamo generator, *Science Reports*, *4*, 3596.

Toh, H., K. Satake, Y. Hamano, Y. Fujii, and T. Goto (2011), Tsunami signals from the 2006 and 2007 Kuril earthquakes detected at a seafloor geomagnetic observatory, *Journal of Geophysical Research*, *116*, B02104.

Tyler, R. H. (2005), A simple formula for estimating the magnetic fields generated by tsunami flow. *Geophysical Research Letters*, *32*, L09608, 4 pp.

Utada, H., H. Shimizu, T. Ogawa, T. Maeda, T. Furumura, T. Yamamoto, N. Yamazaki, Y. Yoshitake and S. Nagamachi (2011), Geomagnetic field changes in response to the 2011 off the Pacific Coast of Tohoku Earthquake and Tsunami, *Earth and Planetary Science Letters*, *311*(1–2), 11–27.

Zhang, L., K. Baba, P. Liang, H. Shimizu, and H. Utada (2014), The 2011 Tohoku tsunami observed by an array of ocean bottom electromagnetometers, *Geophysical Research Letters, 41.*

Table 1. INTERMAGNET and GIS network of geomagnetic observatories used in this work.

IAGA code	Station	country	Geographic coord.	
			Lat.(°)	Long.(°)
CBI[1]	Chichijima	Japan	27.10	142.19
ESA[1]	Esashi	Japan	39.24	141.36
GUA	Guam	United States of America	13.59	144.87
HAR[1]	Haramachi	Japan	37.62	140.95
KAK	Kakioka	Japan	36.23	140.18
KNY	Kanoya	Japan	31.42	130.88
MMB	Memambetsu	Japan	43.92	144.19
OTA[1]	Otaki	Japan	35.29	140.23
TTK[1]	Totsugawa	Japan	33.93	135.80

[1]Observatories belonging to Geospatial Information Authority of Japan (GIS)

Table 2. Simulated locations of the sea surface displacements and distances from the land-ground magnetic observatories.

IAGA code	Distance	Geographic coord.	
		Lat.(°)	Long.(°)
CBI[1]	11 km	27.0	142.19
ESA[1]	43 km	39.1	141.82
GUA	30 km	13.53	144.6
HAR[1]	13 km	37.6	141.1
KAK	36 km	36.2	140.6
KNY	24 km	31.4	131.13
MMB	22 km	44.0	144.43
OTA[1]	35 km	35.52	140.5
TTK[1]	46 km	33.93	136.3

[1]Observatories belonging to Geospatial Information Authority of Japan (GIS)

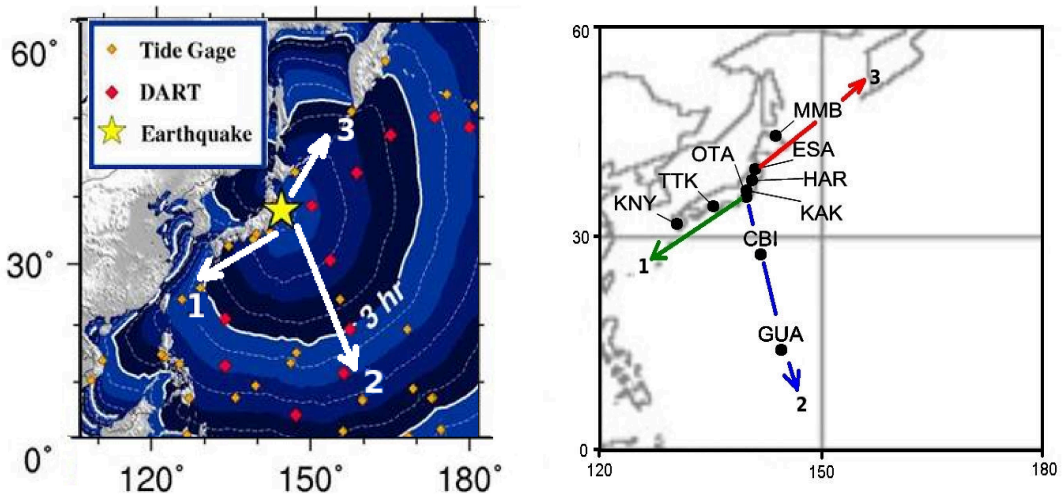

Figure 1. TTT map and map of the geographic localization of the magnetic observatories. TTT map courtesy of NOAA/NWS/West Coast and Alaska Tsunami Warning Center.

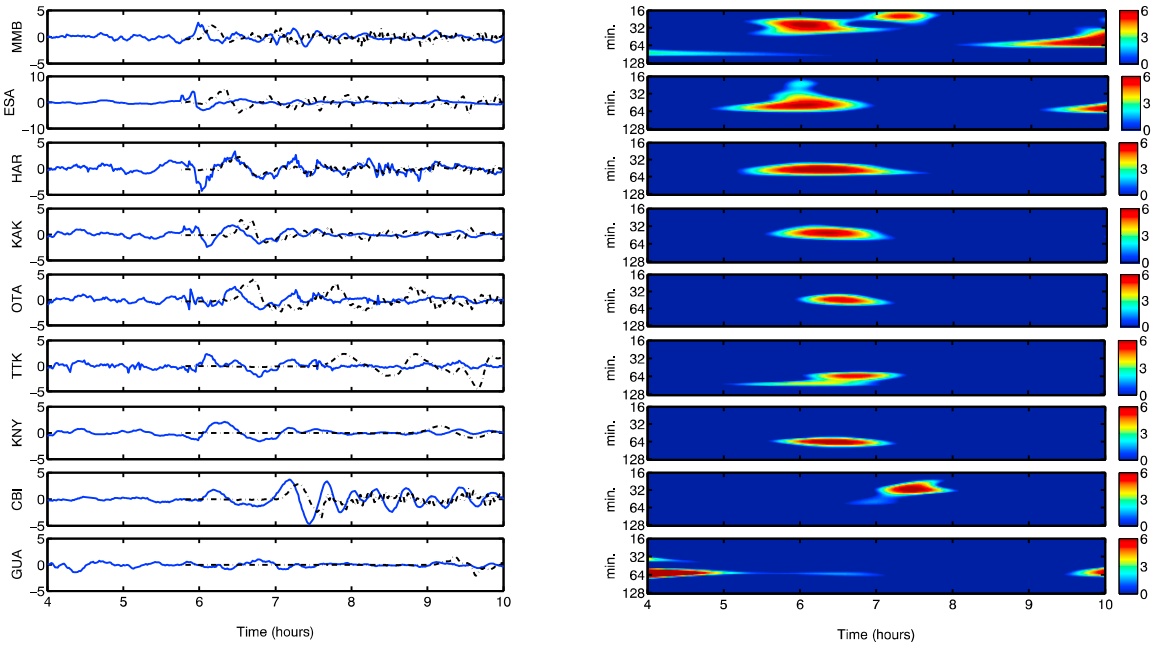

Figure 2. The observed filtered Z-component data (high-pass filter with a cutoff period of 5000s) and wavelet spectral analysis for Japanese event, 2011. Also superimposed is the tsunami wave-field (black color) in the filtered data.

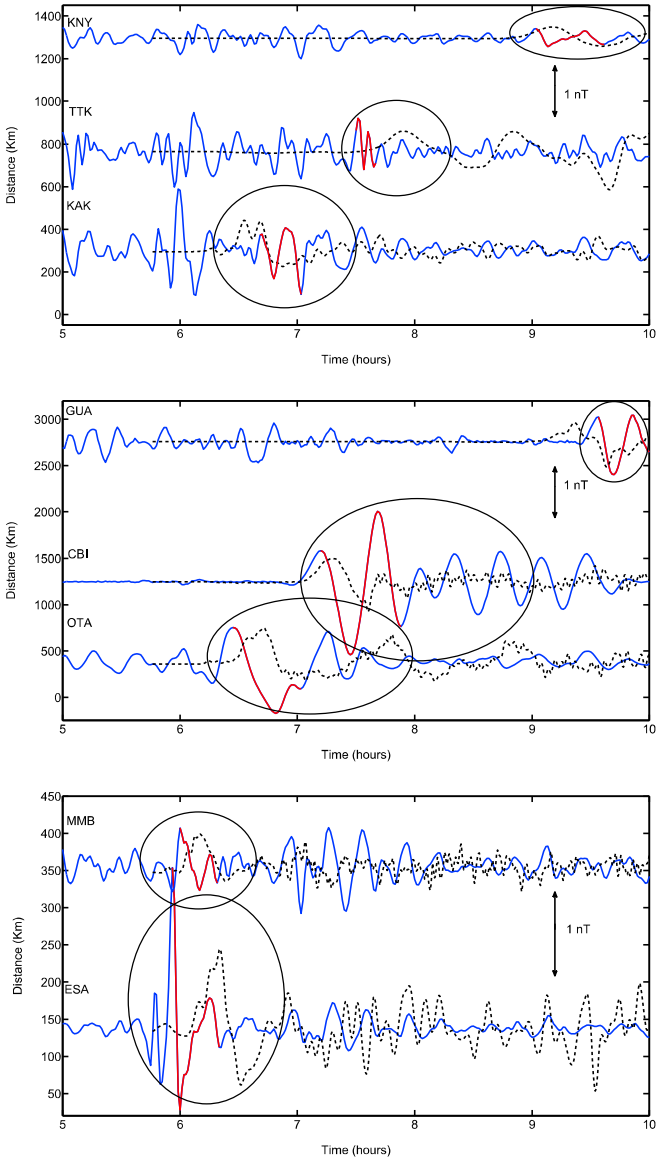

Figure 3. Z-component dataset filtered with a bandpass with periods between 20 and 40 minutes. From left to right, the panels display the TTD on the tsunami propagation direction 1, 2 and 3, respectively. On the vertical axis, it is shown the distance between the earthquake epicenter and the magnetic observatory, and on the horizontal axis, the universal time. The black continued and dot-dashed lines represent the tsunami wave propagation and the tide gauge simulated by tsunami wave model.

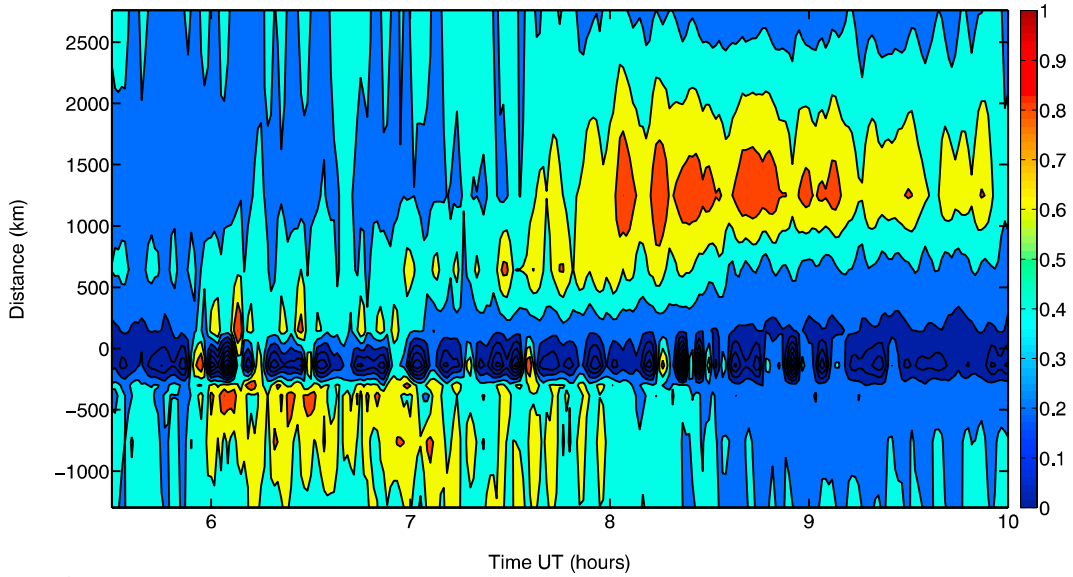

Figure 4. MAPE map between the magnetic observatories along the propagating of the Japanese tsunami wave front.